This article has been accepted for publication in a future issue of this journal, but has not been fully edited. Content may change prior to final publication. Citation information: DOI 10.1109/TAES.2018.2847980, IEEE Transactions on Aerospace and Electronic Systems

Detection Schemes for Range-Spread Targets Based on Semi-Definite Problem

Seungwon Lee, Mai Nguyen, Iickho Song, *Fellow, IEEE*, Jinsoo Bae, *Senior Member, IEEE*, and Seokho Yoon, *Senior Member, IEEE*

***Abstract*—Employing the generalized likelihood ratio test and semi-definite programming (SDP), we derive two detectors, called the SDP and maximization in the reduced space (MRS) detectors for range-spread targets with unknown Doppler shift. It is confirmed that, when knowledge of Doppler frequency is unavailable or imperfect, the proposed detectors perform better than the conventional detector. The MRS detector also outperforms the SDP and conventional detectors in some cases, including when the range-spread target is highly fluctuating.**

***Index Terms*—detection, generalized likelihood ratio test, range-spread target, reduced space, semi-definite programming.**

I. Introduction

In signal detection, we often assume known deterministic, unknown deterministic, and random signals. The known deterministic and random signal models arise rather naturally in a variety of communication problems while various models of deterministic signals with some unknown parameters are frequently encountered in the problems of radar detection [1]–[5]. For radar detection, the generalized likelihood ratio test (GLRT) and Bayesian approaches are commonly employed when the unknown parameter is considered as a deterministic quantity and as the realization of a random variable with a known probability density function (pdf), respectively. When the GLRT is employed, unknown parameters are often replaced by their maximum likelihood estimates (MLE) [6].

In radar detection problems, detection of range-spread targets with an array of antennas has been addressed in a number of studies including [7]–[13], where the target return is in most cases assumed to be known up to a multiplication factor of the steering vector. For instance, in [8] assuming the availability of signal-free data, called the secondary data, the estimation of noise covariance matrix is employed in the detection. In [9], suboptimal invariant receivers have been considered based on the GLRT and principle of invariance. In [11], detection of a range-spread target in spherically invariant random clutter is addressed, and the problem of detecting unknown multidimensional signal in unknown covariance is considered in [12]. In [13], detection of a range-spread target is considered in distributed multiple input multiple output radar when the disturbance covariance matrix exhibits non-homogeneity across transmit-receive antenna pairs.

In the meantime, conventional detection schemes would unavoidably suffer a performance loss when the knowledge about the steering vector is imperfect as in the case of mismatched steering vector. To reduce such a detection loss, detection problems have been addressed under the range models of a linear subspace or a cone class. In essence, the subspace detectors, performing the detection by computing the energy of the measurement in the signal subspace based on linear subspace models, have been considered in [14]–[21]. On the other hand, detectors based on cone class models have been considered in [22]–[26], for example: In most cases of detection under cone class models, likelihood ratios are obtained from numerical methods, and consequently, it is not a simple matter to explain and investigate the nature and performance of detection.

In this paper, we address the detection of a range-spread target in a more general case where the range of steering vector is unknown: The case we consider includes the special case of, for instance, the problem of detecting a target with unknown velocity. We first derive a GLRT based detection scheme for range-spread targets using semi-definite programming (SDP). A simplified detection scheme is then obtained, which possesses an explicit form of the likelihood ratio, and as a consequence, requires much less computational complexity. Both of the proposed detectors are shown to not only have the constant false alarm rate (CFAR) property but also provide, when the Doppler frequency in unknown, a detection performance better than that of the conventional detector derived under the assumption of known Doppler frequency.

II. Problem Formulation and Proposed Detectors

Assume that a potential target is modeled with an unknown range profile (RP) and experiences a motion of unknown velocity relative to the radar. To detect the presence of such a range-spread target, we suppose that the transmitter sends a sequence of N identical coherent pulses of duty cycle T_D with a pulse repetition interval of $T_R \gg T_D$. At the receiver, the reflection from a transmitted pulse is received, passed through a filter matched to the transmit pulse, and then sampled. Here, the reflection of a range-spread target, in case a potential target appears, is assumed to be completely contained in the first L range bins, which is often referred to as the primary data. The secondary data occupies the remaining K range bins and is composed only of noise. Obviously this scenario includes the

Authors' addresses: S. Lee, M. Nguyen, and I. Song are with the School of Electrical Engineering, Korea Advanced Institute of Science and Technology, Daejeon 34141, Korea, E-mail: (kkori21@gmail.com, huongmainuyen12@gmail.com, i.song@ieee.org);

J. Bae is with the College of Electronics and Information Engineering, Sejong University, Seoul 05006, Korea, E-mail: (baej@sejong.ac.kr);

S. Yoon is with the College of Information and Communication Engineering, Sungkyunkwan University, Suwon 16419, Korea, E-mail: (syoon@skku.edu). *(Corresponding author: Seokho Yoon)*

special case of $L = 1$ (*i.e.*, the target is a point scatterer) solved in [27].

Let us denote the sample in the j-th range bin of the t-th pulse by z_{tj} for $t = 1, 2, \ldots, N$ and $j = 1, 2, \ldots, L + K$. If we arrange the samples collected in range bin j over N consecutive pulses, we can form an $N \times 1$ column vector $\boldsymbol{z}_j = [z_{1j}, z_{2j}, \ldots, z_{Nj}]^T$, where $\{\cdot\}^T$ denotes the transpose of a matrix. The detection problem can then be stated as a problem of choosing between the null hypothesis

$$H_0: \quad \boldsymbol{z}_j = \boldsymbol{n}_j, \qquad j = 1, 2, \ldots, L + K, \tag{1}$$

and the alternative hypothesis

$$H_1: \quad \boldsymbol{z}_j = \begin{cases} \alpha_j \boldsymbol{p} + \boldsymbol{n}_j, & j = 1, 2, \ldots, L, \\ \boldsymbol{n}_j, & j = L+1, L+2, \ldots, L+K. \end{cases} \tag{2}$$

In (1) and (2), the null and alternative hypotheses denote the cases of noise-only and signal plus noise observations, respectively; the RP α_j represents the response of scatterers in range bin j and is assumed to be constant during the observation time; and the steering vector

$$\boldsymbol{p} = [1, \exp(j2\pi f_D T_R), \ldots, \exp\{j2\pi f_D (N-1) T_R\}]^T \tag{3}$$

accounts for the Doppler shift with f_D the Doppler frequency. In addition, $\boldsymbol{n}_j$ is an $N \times 1$ zero-mean complex Gaussian noise vector with the common pdf

$$f(\boldsymbol{n}_j) = \frac{1}{\pi^N |\boldsymbol{C}|} \exp\left(-\boldsymbol{n}_j^H \boldsymbol{C}^{-1} \boldsymbol{n}_j\right) \tag{4}$$

for $j = 1, 2, \ldots, L + K$, where the $N \times N$ covariance matrix

$$E\left[\boldsymbol{n}_j \boldsymbol{n}_j^H\right] = \boldsymbol{C} \tag{5}$$

is positive definite and $|\cdot|$ and $\{\cdot\}^H$ denote the determinant and complex conjugate transpose of a matrix, respectively. Note that $\boldsymbol{C}$ is in general a non-diagonal matrix since the sampling interval is short enough in most of practical cases.

Assume that the noise vectors $\{\boldsymbol{n}_i\}_{i=1}^{L+K}$ are identically distributed and independent of each other so that

$$E\left[\boldsymbol{n}_i \boldsymbol{n}_j^H\right] = \boldsymbol{0}_{N \times N} \tag{6}$$

for $i \neq j$, where $\boldsymbol{0}_{a \times b}$ is the $a \times b$ all-zero matrix. The joint pdf of the observed data $\{\boldsymbol{z}_i\}_{i=1}^{L+K}$ can then be expressed as

$$\begin{aligned} f_0(\boldsymbol{z}_1, \boldsymbol{z}_2, \ldots, \boldsymbol{z}_{L+K}) &= \prod_{i=1}^{L+K} f(\boldsymbol{z}_i) \\ &= \frac{1}{(\pi^N |\boldsymbol{C}|)^{L+K}} \exp\left\{-\operatorname{tr}\left(\boldsymbol{C}^{-1} \boldsymbol{T}_0\right)\right\} \end{aligned} \tag{7}$$

and

$$\begin{aligned} &f_1(\boldsymbol{z}_1, \boldsymbol{z}_2, \ldots, \boldsymbol{z}_{L+K}) \\ &= \frac{1}{(\pi^N |\boldsymbol{C}|)^{L+K}} \exp\left\{-\operatorname{tr}\left(\boldsymbol{C}^{-1} \boldsymbol{T}_1\right)\right\} \end{aligned} \tag{8}$$

under H_0 and H_1, respectively, where $\operatorname{tr}(\cdot)$ denotes the trace of a square matrix. In (7) and (8),

$$\boldsymbol{T}_0 = \boldsymbol{R}(\boldsymbol{0}_{L \times 1}) + \boldsymbol{S} \tag{9}$$

and

$$\boldsymbol{T}_1 = \boldsymbol{R}(\boldsymbol{\alpha}) + \boldsymbol{S} \tag{10}$$

represent the 'combined' data, where $\boldsymbol{\alpha} = (\alpha_1, \alpha_2, \ldots, \alpha_L)^T$ is an $L \times 1$ vector composed of the RP,

$$\begin{aligned} \boldsymbol{R}(\boldsymbol{\alpha}) &= \sum_{j=1}^{L} (\boldsymbol{z}_j - \alpha_j \boldsymbol{p})(\boldsymbol{z}_j - \alpha_j \boldsymbol{p})^H \\ &= \left(\boldsymbol{Z} - \boldsymbol{p}\boldsymbol{\alpha}^T\right)\left(\boldsymbol{Z} - \boldsymbol{p}\boldsymbol{\alpha}^T\right)^H \end{aligned} \tag{11}$$

denotes the data in the primary range bins, and the matrix

$$\begin{aligned} \boldsymbol{S} &= \boldsymbol{Z}_S \boldsymbol{Z}_S^H \\ &= \sum_{j=L+1}^{L+K} \boldsymbol{z}_j \boldsymbol{z}_j^H \end{aligned} \tag{12}$$

denotes the secondary data with $\boldsymbol{Z} = [\boldsymbol{z}_1, \boldsymbol{z}_2, \ldots, \boldsymbol{z}_L]$ and $\boldsymbol{Z}_S = [\boldsymbol{z}_{L+1}, \boldsymbol{z}_{L+2}, \ldots, \boldsymbol{z}_{L+K}] = [\boldsymbol{n}_{L+1}, \boldsymbol{n}_{L+2}, \ldots, \boldsymbol{n}_{L+K}]$.

In the sequel, we will employ some fluctuation models for $\boldsymbol{\alpha}$ later in simulations in order to account for the variations of the RP over the L range bins. Clearly $\boldsymbol{R}(\boldsymbol{\alpha})$, $\boldsymbol{S}$, $\boldsymbol{Z}$, and $\boldsymbol{Z}_S$ are of sizes $N \times N$, $N \times N$, $N \times L$, and $N \times K$, respectively. Note that the matrix $\boldsymbol{S}$ is positive semi-definite Hermitian: In addition, it is a non-singular matrix with probability one when $K \gg N$. Thus, the matrix $\boldsymbol{S}$ can be regarded positive definite Hermitian without loss of generality.

From the Neyman-Pearson criterion, the likelihood ratio test (LRT) for the problem of choosing between H_0 and H_1 can now be expressed as

$$\frac{\max\limits_{\boldsymbol{p}} \max\limits_{\boldsymbol{\alpha}} \max\limits_{\boldsymbol{C}} f_1(\boldsymbol{z}_1, \boldsymbol{z}_2, \ldots, \boldsymbol{z}_{L+K})}{\max\limits_{\boldsymbol{C}} f_0(\boldsymbol{z}_1, \boldsymbol{z}_2, \ldots, \boldsymbol{z}_{L+K})} \underset{H_0}{\overset{H_1}{\gtrless}} G, \tag{13}$$

where the threshold G is chosen based on a desired false alarm rate. When the noise covariance matrix $\boldsymbol{C}$, RP $\boldsymbol{\alpha}$ of the target, and Doppler shift vector $\boldsymbol{p}$ are unavailable, a direct derivation of the LRT is not possible and we resort to a GLRT scheme, replacing nuisance parameters with their MLEs under each hypothesis. Now, as it is well-known, the MLE of the noise covariance matrix $\boldsymbol{C}$ under H_i is $\boldsymbol{T}_i$ for $i = 0$ and 1. If we substitute the noise covariance matrix $\boldsymbol{C}$ in (13) with the MLEs, we will be led to

$$\frac{|\boldsymbol{T}_0|}{\min\limits_{\boldsymbol{p}} \min\limits_{\boldsymbol{\alpha}} |\boldsymbol{T}_1|} \underset{H_0}{\overset{H_1}{\gtrless}} G_1, \tag{14}$$

where $G_1 = \ln G$. The minimization in the denominator over the RP vector $\boldsymbol{\alpha}$ can subsequently be attained for [28]

$$\hat{\boldsymbol{\alpha}} = \kappa(\boldsymbol{p}) \left(\boldsymbol{p}^H \boldsymbol{S}^{-1} \boldsymbol{Z}\right)^T, \tag{15}$$

where

$$\kappa(\boldsymbol{p}) = \frac{1}{\boldsymbol{p}^H \boldsymbol{S}^{-1} \boldsymbol{p}} \tag{16}$$

is a positive number since $\boldsymbol{S}^{-1}$ is a positive definite matrix. Hence, the GLRT (14) can further be rewritten as

$$\frac{|\boldsymbol{R}(\boldsymbol{0}_{L \times 1}) + \boldsymbol{S}|}{\min\limits_{\boldsymbol{p}} |\boldsymbol{R}(\hat{\boldsymbol{\alpha}}) + \boldsymbol{S}|} \underset{H_0}{\overset{H_1}{\gtrless}} G_1. \tag{17}$$

After some manipulations as shown in Appendix A, the GLRT (17) is eventually recast as

$$t^{\dagger} \underset{H_0}{\overset{H_1}{\gtrless}} G_2, \tag{18}$$

where

$$t^{\dagger} = \max_{\boldsymbol{p}} \kappa(\boldsymbol{p}) \boldsymbol{p}^H \boldsymbol{S}^{-1} \boldsymbol{Z} \boldsymbol{X}^{-1} \boldsymbol{Z}^H \boldsymbol{S}^{-1} \boldsymbol{p}, \tag{19}$$

G_2 is a suitable modification of G_1, and $\boldsymbol{p}$ is an optimization variable. In (19), we have

$$\boldsymbol{X} = \boldsymbol{I}_L + \boldsymbol{\Upsilon}, \tag{20}$$

where $\boldsymbol{I}_L$ is the $L \times L$ identity matrix and

$$\boldsymbol{\Upsilon} = \boldsymbol{Z}^H \boldsymbol{S}^{-1} \boldsymbol{Z}. \tag{21}$$

Clearly, the quantity $t^{\dagger}$ is non-negative since the matrix $\boldsymbol{S}^{-1} \boldsymbol{Z} \boldsymbol{X}^{-1} \boldsymbol{Z}^H \boldsymbol{S}^{-1}$ is positive semi-definite and $\kappa(\boldsymbol{p})$ is positive. Let us also note in passing that, when $\boldsymbol{p}$ is known, a GLRT similar to (18) is addressed in [8].

A. Detector based on Semi-Definite Problem

When $\boldsymbol{p}$ is unknown, the maximization in (19) can theoretically be solved by searching over $\boldsymbol{p}$: Unfortunately, such a scheme is not quite feasible in practice. We thus change (19) into an equivalent problem for which efficient algorithms can be employed.

Recollecting that $\boldsymbol{p} = [1, \exp(j\theta), \ldots, \exp\{j(N-1)\theta\}]^T$ with $\theta = 2\pi f_D T_R \in [0, 2\pi)$ the Doppler phase, let us first rewrite (19) as

$$\begin{array}{ll} \text{minimize} & t \\ \text{subject to} & f(\theta, t) \geqslant 0, \end{array} \tag{22}$$

where

$$f(\theta, t) = t y_0 - x_0 + 2\mathcal{R}e\left\{\sum_{k=1}^{N-1} (t y_k - x_k) \exp(jk\theta)\right\}, \tag{23}$$

and θ and t are optimization variables with $\mathcal{R}e\{\cdot\}$ denoting the real part. More details on the steps leading from (19) to (22) and (23) are depicted in Appendix B. In (23), we have

$$x_k = \sum_{n-m=k} \left(\boldsymbol{S}^{-1} \boldsymbol{Z} \boldsymbol{X}^{-1} \boldsymbol{Z}^H \boldsymbol{S}^{-1}\right)_{mn} \tag{24}$$

and

$$y_k = \sum_{n-m=k} \left(\boldsymbol{S}^{-1}\right)_{mn} \tag{25}$$

for $k = 0, 1, \ldots, N-1$, where $(\cdot)_{mn}$ denotes the elements at the m-th row and n-th column of a matrix. Let us mention that x_k and y_k are the sums of the upper diagonal elements of the matrices $\boldsymbol{S}^{-1} \boldsymbol{Z} \boldsymbol{X}^{-1} \boldsymbol{Z}^H \boldsymbol{S}^{-1}$ and $\boldsymbol{S}^{-1}$, respectively, such that the column index is larger than the row index by k for $k = 1, 2, ..., N-1$ and that $x_0 = \operatorname{tr}\left(\boldsymbol{S}^{-1} \boldsymbol{Z} \boldsymbol{X}^{-1} \boldsymbol{Z}^H \boldsymbol{S}^{-1}\right)$ and $y_0 = \operatorname{tr}\left(\boldsymbol{S}^{-1}\right)$, sums of diagonal elements, are both real numbers since $\boldsymbol{S}^{-1} \boldsymbol{Z} \boldsymbol{X}^{-1} \boldsymbol{Z}^H \boldsymbol{S}^{-1}$ and $\boldsymbol{S}^{-1}$ are Hermitian matrices. Note that the constraint $f(\theta, t) \geqslant 0$ is derived from, and therefore equivalent to,

$$t - \kappa(\boldsymbol{p}) \boldsymbol{p}^H \boldsymbol{S}^{-1} \boldsymbol{Z} \boldsymbol{X}^{-1} \boldsymbol{Z}^H \boldsymbol{S}^{-1} \boldsymbol{p} \geqslant 0. \tag{26}$$

We observe that if $f(\theta, t) \geqslant 0 \text{ over } \theta \in [0, 2\pi)$ then $t \geqslant t^{\dagger}$ and vice versa. In other words, the set $\{t : t \geqslant t^{\dagger}\}$ of t is the same as the set $\{t : f(\theta, t) \geqslant 0, \theta \in [0, 2\pi)\}$ of t. Hence, the solution to the problem (22) is the minimum among the values of t making $f(\theta, t)$ non-negative over $[0, 2\pi)$: To find the minimum, we apply the following result, modified from a theorem in [29] by replacing the variable x_k with $t y_k - x_k$. A detailed proof is omitted here due to lack of space.

Theorem 1. *The function $f(\theta, t)$ is non-negative over $[0, 2\pi)$ if and only if there exists a matrix $\boldsymbol{V} \in \mathbb{H}^{N \times N}$ such that*

$$t\boldsymbol{y} - \boldsymbol{x} = \boldsymbol{W}^H \operatorname{diag}\left(\boldsymbol{W} \boldsymbol{V} \boldsymbol{W}^H\right). \tag{27}$$

Here, $\mathbb{H}^{N \times N}$ denotes the set of $N \times N$ non-negative definite Hermitian matrices, $\boldsymbol{y} = [y_0, y_1, \ldots, y_{N-1}]^T$, $\boldsymbol{x} = [x_0, x_1, \ldots, x_{N-1}]^T$, $\operatorname{diag}(\cdot)$ denotes the $N \times 1$ vector formed with the diagonal elements, and

$$\boldsymbol{W} = [\boldsymbol{w}_0, \boldsymbol{w}_1, \ldots, \boldsymbol{w}_{N-1}] \tag{28}$$

is an $N \times N$ matrix, where $\boldsymbol{w}_i = \left[1, \omega_{M,i}, \ldots, \omega_{M,i}^{N-1}\right]^T$ with

$$\omega_{M,i} = \exp\left(-j\frac{2\pi i}{M}\right) \tag{29}$$

for $i = 0, 1, \ldots, N-1$ and M a number satisfying $M \geqslant 2N-1$.

The minimization (22) can finally be expressed as

$$\begin{array}{ll} \text{minimize} & t \\ \text{subject to} & t\boldsymbol{y} - \boldsymbol{x} = \boldsymbol{W}^H \operatorname{diag}\left(\boldsymbol{W} \boldsymbol{V} \boldsymbol{W}^H\right), \\ & \boldsymbol{V} \in \mathbb{H}^{N \times N} \end{array} \tag{30}$$

by applying Theorem 1, where $\boldsymbol{V}$ and t are optimization variables. Since the minimization problem of (30) is a semi-definite problem, a class of convex optimization problems, it can be solved efficiently by various well-known methods such as the interior-point, first-order, and bundle methods [30].

The resulting detector, which will be called the SDP detector in this paper, eventually assumes the LRT

$$t_C \underset{H_0}{\overset{H_1}{\gtrless}} G_2, \tag{31}$$

where t_C is the solution of (30) obtained by, for example, the interior-point method.

Theoretically, the performance of the detector (31) would be the same as that of (18). On the other hand, the performance of (18) will in practice depend on the resolution of the searching grid of θ (or equivalently, the unknown Doppler frequency) while the detector (31) is less dependent on the resolution of the searching grid: In addition, various efficient algorithms can be employed in solving (31) as mentioned above. Let us note that the study in [31] also applied the result in [29], but unlike in our work, for the detection of 'point-like' targets in uncorrelated Gaussian noise under unknown direction of arrival.

B. Detector based on Maximization in Reduced Space

When the likelihood ratio t_C is obtained from (30) via the SDP, the processing time will increase as the number of range bins (that is, with the range resolution of the radar) as in other schemes. In addition, the likelihood ratio t_C does not possess an explicit expression, not allowing any insight into the performance characteristics.

To alleviate the drawbacks of t_C, we now attempt to derive a detector by replacing the search over $\boldsymbol{p}$ with the search over all $N \times 1$ complex vectors. With this relaxation, we can move a few steps further in simplifying, and explicitly showing, the structure of the detector. Of course, since we do not exploit *a priori* knowledge about $\boldsymbol{p}$, the simplification is achieved at the expense of some performance loss.

From the unitary similarity [32], we have

$$\boldsymbol{S}^{-1} = \boldsymbol{U}_{S^{-1}}^{H} \boldsymbol{\Lambda}_{S^{-1}} \boldsymbol{U}_{S^{-1}} \tag{32}$$

since $\boldsymbol{S}^{-1}$ is a Hermitian matrix, where $\boldsymbol{U}_{S^{-1}}$ is an $N \times N$ unitary matrix such that $\boldsymbol{U}_{S^{-1}}^{H} = \boldsymbol{U}_{S^{-1}}^{-1}$ and $\boldsymbol{\Lambda}_{S^{-1}} = \text{diag}\,(\lambda_i)$ with $\{\lambda_i\}_{i=1}^{N}$ the eigenvalues of $\boldsymbol{S}^{-1}$. Note that $\{\lambda_i\}_{i=1}^{N}$ are all positive with probability one since $\boldsymbol{S}^{-1}$ is a positive definite matrix with probability one. Defining the $N \times 1$ vector

$$\boldsymbol{l} = \boldsymbol{\Lambda}_{S^{-1}}^{1/2} \boldsymbol{U}_{S^{-1}} \boldsymbol{p} \tag{33}$$

and $N \times L$ matrix

$$\boldsymbol{Y} = \boldsymbol{\Lambda}_{S^{-1}}^{1/2} \boldsymbol{U}_{S^{-1}} \boldsymbol{Z}, \tag{34}$$

we have

$$\boldsymbol{l}^{H} \boldsymbol{l} = \boldsymbol{p}^{H} \boldsymbol{S}^{-1} \boldsymbol{p} = \frac{1}{\kappa\,(\boldsymbol{p})} \tag{35}$$

and

$$\boldsymbol{l}^{H} \boldsymbol{Y} = \boldsymbol{p}^{H} \boldsymbol{S}^{-1} \boldsymbol{Z}, \tag{36}$$

where $\boldsymbol{\Lambda}_{S^{-1}}^{1/2} = \text{diag}\left(\sqrt{\lambda_i}\right)$. Thus, the right-hand side in (19) can be rewritten as

$$\max_{\boldsymbol{l}} \frac{\boldsymbol{l}^{H} \boldsymbol{Y} \left(\boldsymbol{I}_L + \boldsymbol{\Upsilon}\right)^{-1} \boldsymbol{Y}^{H} \boldsymbol{l}}{\boldsymbol{l}^{H} \boldsymbol{l}}. \tag{37}$$

Here, it should be noticed that the ratio in (37) is the Rayleigh quotient [33] of the Hermitian matrix $\boldsymbol{Y}\left(\boldsymbol{I}_L + \boldsymbol{\Upsilon}\right)^{-1} \boldsymbol{Y}^{H}$ at $\boldsymbol{l}$: An important implication of this fact is that the maximum of the ratio, or equivalently the solution to (37) over all $N \times 1$ vectors, is the same as the maximum of the eigenvalues of the Hermitian matrix $\boldsymbol{Y}\left(\boldsymbol{I}_L + \boldsymbol{\Upsilon}\right)^{-1} \boldsymbol{Y}^{H}$.

Now, denoting the set of non-zero eigenvalues by $\text{eig}\{\cdot\}$, we have

$$\begin{aligned} \text{eig}\left\{\boldsymbol{Y}\left(\boldsymbol{I}_L + \boldsymbol{\Upsilon}\right)^{-1} \boldsymbol{Y}^{H}\right\} &= \text{eig}\left\{\left(\boldsymbol{I}_L + \boldsymbol{\Upsilon}\right)^{-1} \boldsymbol{Y}^{H} \boldsymbol{Y}\right\} \\ &= \text{eig}\left\{\left(\boldsymbol{I}_L + \boldsymbol{\Upsilon}\right)^{-1} \boldsymbol{\Upsilon}\right\}, \end{aligned} \tag{38}$$

where the first equality is based on the fact that $\text{eig}\{\boldsymbol{AB}\} = \text{eig}\{\boldsymbol{BA}\}$ for any $m \times n$ matrix $\boldsymbol{A}$ and $n \times m$ matrix $\boldsymbol{B}$ [34] and the second equality is from $\boldsymbol{Y}^{H}\boldsymbol{Y} = \left(\boldsymbol{\Lambda}_{S^{-1}}^{1/2} \boldsymbol{U}_{S^{-1}} \boldsymbol{Z}\right)^{H} \boldsymbol{\Lambda}_{S^{-1}}^{1/2} \boldsymbol{U}_{S^{-1}} \boldsymbol{Z} = \boldsymbol{Z}^{H} \boldsymbol{U}_{S^{-1}}^{H} \left(\boldsymbol{\Lambda}_{S^{-1}}^{1/2}\right)^{H} \boldsymbol{\Lambda}_{S^{-1}}^{1/2} \boldsymbol{U}_{S^{-1}} \boldsymbol{Z} = \boldsymbol{\Upsilon}$. Since $\boldsymbol{\Upsilon} = \boldsymbol{Z}^{H} \boldsymbol{S}^{-1} \boldsymbol{Z}$ is a Hermitian matrix, we have the decomposition

$$\boldsymbol{\Upsilon} = \boldsymbol{U}_{\Upsilon}^{H} \boldsymbol{\Lambda}_{\Upsilon} \boldsymbol{U}_{\Upsilon}, \tag{39}$$

where $\boldsymbol{U}_{\Upsilon}$ is an $L \times L$ unitary matrix and $\boldsymbol{\Lambda}_{\Upsilon}$ is the $L \times L$ diagonal matrix composed of the eigenvalues

$$\text{eig}\{\boldsymbol{\Upsilon}\} = \{d_i\}_{i=1}^{L} \tag{40}$$

of $\boldsymbol{\Upsilon}$. Thus, we get

$$\begin{aligned} &\text{eig}\left\{\left(\boldsymbol{I}_L + \boldsymbol{\Upsilon}\right)^{-1} \boldsymbol{\Upsilon}\right\} \\ &= \text{eig}\left\{\left(\boldsymbol{I}_L + \boldsymbol{U}_{\Upsilon}^{H} \boldsymbol{\Lambda}_{\Upsilon} \boldsymbol{U}_{\Upsilon}\right)^{-1} \boldsymbol{U}_{\Upsilon}^{H} \boldsymbol{\Lambda}_{\Upsilon} \boldsymbol{U}_{\Upsilon}\right\} \\ &= \text{eig}\left\{\left[\boldsymbol{U}_{\Upsilon}^{H} \left(\boldsymbol{I}_L + \boldsymbol{\Lambda}_{\Upsilon}\right) \boldsymbol{U}_{\Upsilon}\right]^{-1} \boldsymbol{U}_{\Upsilon}^{H} \boldsymbol{\Lambda}_{\Upsilon} \boldsymbol{U}_{\Upsilon}\right\} \\ &= \text{eig}\left\{\boldsymbol{U}_{\Upsilon}^{H} \left(\boldsymbol{I}_L + \boldsymbol{\Lambda}_{\Upsilon}\right)^{-1} \boldsymbol{\Lambda}_{\Upsilon} \boldsymbol{U}_{\Upsilon}\right\} \\ &= \text{eig}\left\{\left(\boldsymbol{I}_L + \boldsymbol{\Lambda}_{\Upsilon}\right)^{-1} \boldsymbol{\Lambda}_{\Upsilon}\right\}, \end{aligned} \tag{41}$$

where we have used $\boldsymbol{U}_{\Upsilon}^{-1} = \boldsymbol{U}_{\Upsilon}^{H}$ in the third equality and the last equality is based on the fact that $\text{eig}\{\boldsymbol{A}\} = \text{eig}\left\{\boldsymbol{B}^{-1}\boldsymbol{AB}\right\}$ when $\boldsymbol{A}$ and $\boldsymbol{B}$ are square matrices of the same size and $\boldsymbol{B}$ is an invertible matrix [32].

The matrix $\left(\boldsymbol{I}_L + \boldsymbol{\Lambda}_{\Upsilon}\right)^{-1} \boldsymbol{\Lambda}_{\Upsilon}$ is a diagonal matrix, and therefore, its eigenvalues are the same as its elements $\left\{\frac{d_i}{1+d_i}\right\}_{i=1}^{L}$ since $\boldsymbol{\Upsilon}$ is a positive semi-definite matrix, where $d_i \geq 0$ for $i = 1, 2, \ldots, L$. Noting that $\frac{x}{1+x}$ is an increasing function of $x \geq 0$, it is easy to see that the maximum eigenvalue of $\left(\boldsymbol{I}_L + \boldsymbol{\Lambda}_{\Upsilon}\right)^{-1} \boldsymbol{\Lambda}_{\Upsilon}$, or equivalently the maximum value of (37), is $\frac{d_{\max}}{1+d_{\max}}$, where

$$d_{\max} = \max\{d_1, d_2, \ldots, d_L\}. \tag{42}$$

In passing, let us just note that the largest order statistic [35], [36] is also useful in various applications including, for example, in the study of flooding.

The resulting detector, which we will call the maximization in the relaxed space (MRS) detector, is thus based on the LRT

$$\frac{d_{\max}}{1+d_{\max}} \underset{H_0}{\overset{H_1}{\gtrless}} \tilde{G}_2, \tag{43}$$

where $\tilde{G}_2$ is the threshold. We have shown in Appendix C that the MRS detector (43) possesses a CFAR property.

III. Simulation Results

In this section, let us assess and compare the performance, the probabilities of detection and false alarm, of the proposed detectors (31) and (43) with that of the conventional detector

$$\frac{\boldsymbol{p}^{H} \boldsymbol{S}^{-1} \boldsymbol{Z} \boldsymbol{X}^{-1} \boldsymbol{Z}^{H} \boldsymbol{S}^{-1} \boldsymbol{p}}{\boldsymbol{p}^{H} \boldsymbol{S}^{-1} \boldsymbol{p}} \underset{H_0}{\overset{H_1}{\gtrless}} \tilde{G}_3 \tag{44}$$

derived under the assumption of known $\boldsymbol{p}$, where $\tilde{G}_3$ is the threshold. The detector represented by (44) will be called the one-step GLRT (OS-GLRT) [8].

This article has been accepted for publication in a future issue of this journal, but has not been fully edited. Content may change prior to final publication. Citation information: DOI 10.1109/TAES.2018.2847980, IEEE Transactions on Aerospace and Electronic Systems

TABLE I
ENERGY DISTRIBUTION AT DISCRETE SCATTERER LOCATIONS WHEN $L = 8$, 12, 16, AND 20

$L = 8$	0	$\frac{1}{16}$	0	$\frac{1}{2}$	$\frac{1}{4}$	$\frac{1}{16}$	$\frac{1}{8}$	0												
$L = 12$	0	$\frac{1}{16}$	$\frac{1}{16}$	0	0	0	$\frac{1}{16}$	$\frac{1}{16}$	$\frac{1}{2}$	$\frac{1}{4}$	0	0								
$L = 16$	0	0	$\frac{1}{32}$	$\frac{1}{32}$	0	$\frac{1}{2}$	$\frac{1}{4}$	0	$\frac{1}{32}$	0	$\frac{1}{16}$	$\frac{1}{32}$	0	$\frac{1}{16}$	0	0				
$L = 20$	0	$\frac{1}{10}$	0	$\frac{1}{10}$	0	$\frac{1}{10}$	0	$\frac{1}{10}$	0	$\frac{1}{10}$	0	$\frac{1}{10}$	0	$\frac{1}{10}$	0	$\frac{1}{10}$	0	$\frac{1}{10}$	0	$\frac{1}{10}$

A. Simulation Parameters

We assume $N = 8$ identical coherent pulses transmitted with the pulse repetition interval $T_R = 40$ μs and Doppler frequency $f_D = 10$ kHz (which corresponds to a velocity of 150 m/s for a wavelength of $\lambda = 3$ cm). The number L of range cells in the primary data is lower bounded by the ratio of the range extent of a target to the range resolution of a radar and it could be of several hundreds. To alleviate the computational burden, we have chosen $L = 8, 12, 16$, and 20 with the energy distribution among scatterers as shown in Table I. The size of secondary data is chosen as $K = 16N = 128$ so that the matrix $\boldsymbol{S}$ of secondary data is non-singular. For use in (28), we have chosen $M = 2N - 1 = 15$. We assume that the numbers L and K are accurately known to detectors ahead of time as are in other studies, *e.g.*, [9]. Finally, we use the software CVX (http://cvxr.com/) to solve (30) on a computer equipped with a 3.4 GHz Intel processor.

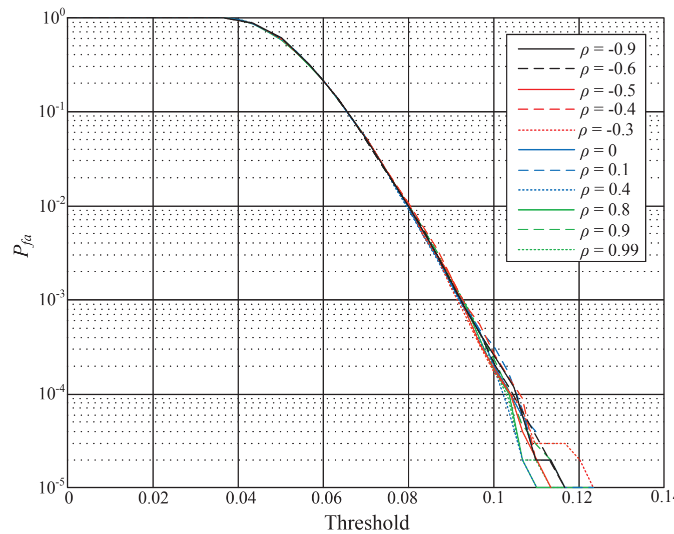

Fig. 1. False alarm probability versus thresholds of the SDP detector.

B. Simulation Results and Discussion

The performance of the SDP and MRS detectors are assessed in comparison with the OS-GLRT detector for the detection of steady and fluctuating targets embedded in Gaussian noise of various degrees of correlation. In addition, the complexities of the three detectors are investigated.

Since it is not plausible to derive explicit expressions of the false alarm and detection probabilities, we resort to Monte Carlo trials, in which the detection probability is obtained when the false alarm rate is set at 10^{-4}. As shown in Appendix C and in [8], respectively, the MRS and OS-GLRT detectors are CFAR detectors. Based on this observation, the thresholds of the MRS and OS-GLRT detectors are determined once.

1) Threshold of the SDP detector: We first investigate if the SDP detector also has a CFAR property under the assumption that the noise vectors have the covariance matrix

$$\boldsymbol{C} = \sigma_n^2 \begin{bmatrix} 1 & \rho & \dots & \rho^{N-1} \\ \rho & 1 & \dots & \rho^{N-2} \\ \vdots & \vdots & \ddots & \vdots \\ \rho^{N-1} & \rho^{N-2} & \dots & 1 \end{bmatrix}, \tag{45}$$

where σ_n^2 and ρ denote the average noise power in one range cell and one-lag correlation coefficient, respectively.

The false alarm rate of the SDP detector is shown in Figure 1 as a function of threshold for various values of ρ when $\sigma_n^2 = 1$. It is clear that the threshold does not depend on ρ, which we believe is a natural consequence since the likelihood ratio of the SDP detector is a close approximation to that of the OS-GLRT detector, a CFAR detector.

2) Detection performance with steady targets: First, let us evaluate the detection performance when the RP of a potential target remains constant during the observation time. For $L = 8$ and $\rho = 0.4$, we assume target velocity $v = -100$, 120, 150, and 180 m/s, which correspond to Doppler frequency $f_D = -6.67$, 8, 10, and 12 kHz, respectively.

Figure 2 shows the detection probability as a function of the signal-to-noise ratio (SNR) defined as

$$\mathrm{SNR} = \frac{\|\boldsymbol{p}\|^2 \sum\limits_{i=1}^{L} |\alpha_i|^2}{LN\sigma_n^2}. \tag{46}$$

It is clearly indicated that the SDP detector achieves nearly the same performance as the OS-GLRT detector and outperforms the MRS detector. For example, the SDP detector provides a gain of around 1.4 dB over the MRS detector for all the values of f_D.

The detection probability is next assessed when $\rho = -0.9$, -0.4, 0, 0.4, and 0.9 for $L = 8$ as shown in Figure 3. It is observed that the SDP detector performs close to, and better than, the OS-GLRT and MRS detectors, respectively: It should again be recollected that, unlike the OS-GLRT detector, the

This article has been accepted for publication in a future issue of this journal, but has not been fully edited. Content may change prior to final publication. Citation information: DOI 10.1109/TAES.2018.2847980, IEEE Transactions on Aerospace and Electronic Systems

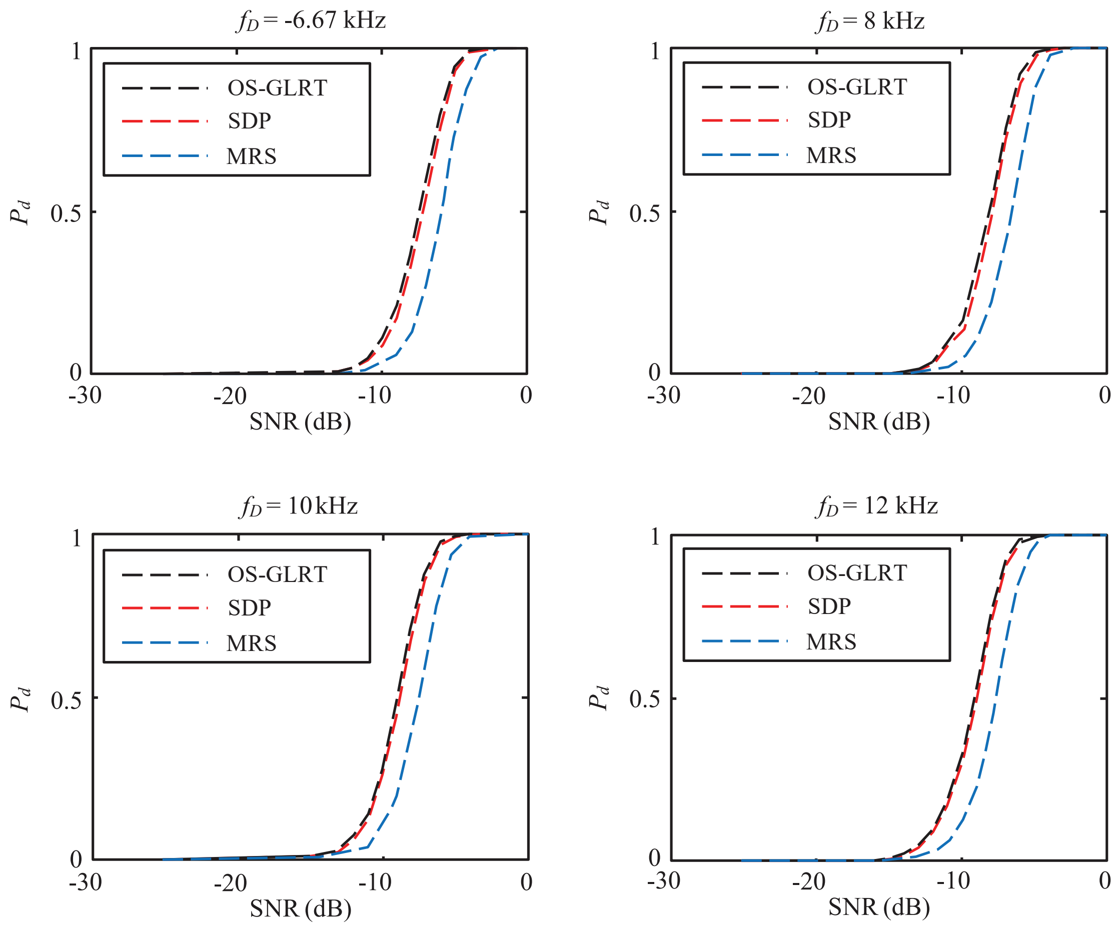

Fig. 2. Detection probability of the OS-GLRT, SDP, and MRS detectors for steady target.

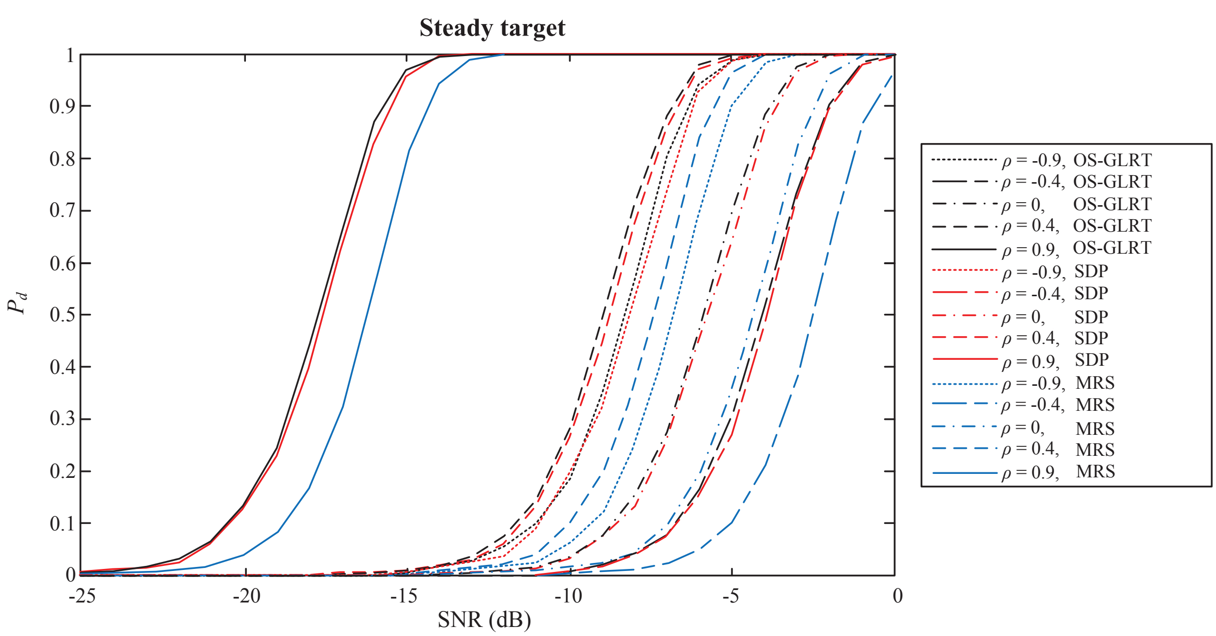

Fig. 3. Detection probability of the OS-GLRT, SDP, and MRS detectors for steady target.

This article has been accepted for publication in a future issue of this journal, but has not been fully edited. Content may change prior to final publication. Citation information: DOI 10.1109/TAES.2018.2847980, IEEE Transactions on Aerospace and Electronic Systems

TABLE II
AVERAGE COMPUTATIONAL TIME (IN SECOND) OF OS-GLRT, SDP, AND MRS DETECTORS

	$L = 8$	$L = 12$	$L = 16$	$L = 20$
OS-GLRT	2.44×10^{-4}	2.85×10^{-4}	3.32×10^{-4}	3.88×10^{-4}
SDP	1.53×10^{-1}	1.59×10^{-1}	2.01×10^{-1}	2.03×10^{-1}
MRS	3.55×10^{-4}	3.63×10^{-4}	4.87×10^{-4}	6.12×10^{-4}

SDP and MRS detectors do not require information on Doppler frequency.

3) Detection performance with fluctuating targets: Next, let us investigate the detection performance when the RP of a potential target fluctuates. In the detection of fluctuating targets, the sum of energy from the main scatterer is normally considered as the total energy returned from the target [5], and is represented by the radar cross section (RCS). For simplicity in the modeling, we assume that all the RP's $\{|\alpha_j|\}_{j=1}^{L}$ follow the same fluctuation pattern of the RCS described by Swerling models [37].

With a fluctuation model of the RCS, the SNR can be expressed as

$$\begin{aligned} \mathrm{SNR}_{fluct} &= \frac{E\left[\|\boldsymbol{p}\|^2 \sum\limits_{i=1}^{L} |\alpha_i|^2\right]}{LN\sigma_n^2} \\ &\propto \frac{\bar{\sigma}\|\boldsymbol{p}\|^2}{LN\sigma_n^2}, \end{aligned} \tag{47}$$

where $fluct$ stands for 'fluctuation' and $\bar{\sigma}$ denotes the average RCS with the RCS proportional to $\sum\limits_{j=1}^{L} |\alpha_j|^2$. Note that Swerling II and IV models are basically χ^2 distributions with degrees of freedom 2 and 4, respectively: At the same expected value, a Swerling II variable exhibits a larger covariance (more fluctuation) than a Swerling IV variable.

Figures 4 and 5 show the detection probabilities as functions of the SNR for Swerling IV and II targets, respectively. In detecting Swerling IV targets, the SDP detector in most cases performs almost the same as the OS-GLRT detector and better than the MRS detector, and outperforms the OS-GLRT detector in some environment (that is, when the noise correlation is of high negative value). In addition, for the detection of Swerling II targets (in other words, when the degree of fluctuation of the target is higher), we have a similar observation but with an exception that the MRS detector now becomes the most effective scheme among the three detectors when the noise correlation is of high negative value: There could be many explanations for this. One possibility is that the return signal from a fluctuating target, when combined with noise of high negative correlation, is matched better to the model of an arbitrary $\boldsymbol{p}$ employed in the MRS detector than to the model of a sinusoidal $\boldsymbol{p}$ employed in the SDP and detector to the model of fixed $\boldsymbol{p}$ employed in the OS-GLRT detector.

4) Detection with incorrect information about Doppler frequency: Figure 6 shows the detection performance for $L = 8$, $\rho = 0.4$, and a steady RP when Doppler frequency is incorrectly assumed as 10 kHz while the actual value is 12 kHz. It is clearly observed that the SDP and MRS detectors outperform the OS-GLRT detector, implying some robustness property for the SDP and MRS detectors: This is not an unexpected observation since the SDP and MRS detectors do not require the availability of Doppler frequency while the OS-GLRT detector requires exact information about Doppler frequency.

5) Complexity of proposed detectors: Let us now consider the complexity in theory and that in terms of average time consumption. For the SDP detector, the interior-point method converges in $\mathcal{O}\left(\sqrt{N}\log(1/\epsilon)\right)$ iterations within a tolerance ϵ [38] and each main iteration involves $\mathcal{O}\left(N^6\right)$ to solve the optimization problem. Hence, interior-point SDP solvers have a computational complexity of $\mathcal{O}\left(N^{6.5}\right)$. Dominated by eigen-decomposition, the computational complexity of the MRS detector is $\mathcal{O}\left(bL^3\right)$, where b denotes the number of iterations required for convergence with a typical value of $20 \sim 30$ [39], [40]. Note that b does not depend on the size N of data. The computational complexity of the OS-GLRT detector is known to be $\mathcal{O}\left(KN^2\right) + \mathcal{O}\left(L^3\right) + \mathcal{O}\left(L^2N\right)$ [8].

Next, let us consider the complexity in terms of average time consumption, where the averaging is executed over 1000 repetitions to make the results significant enough. We have obtained the average time consumed for four values 8, 12, 16, and 20 of the length L of RP. As easily anticipated, Table II shows that the SDP detector, solving (30), consumes much more processing time (in the order of 10^{-1} second) than the MRS and OS-GLRT detectors (in the order of 10^{-4} second), which is the cost we pay to detect range-spread targets without exact information on the Doppler frequency. Interestingly, computing the maximum eigenvalue of $\boldsymbol{Z}^H\boldsymbol{S}^{-1}\boldsymbol{Z}$, the MRS detector designed to detect range-spread targets without requiring exact information on the Doppler frequency consumes only slightly more time than the OS-GLRT detector designed to detect range-fixed targets.

6) Performance in detecting multiple range-spread targets: Let us discuss briefly the performance of detectors for the detection of multiple range-spread targets. Although we have not shown explicitly in this paper, when the Doppler shift is unknown, both the SDP and MRS detectors are expected to outperform the conventional detector for the detection of multiple range-spread targets also. Of course, in the detection of multiple range-spread targets, the complexity requirement of any detector would be higher than that in the detection of single range-spread target. If the multiple range-spread targets are correlated in addition, the detection complexity will become very high, in which case we might also need to take the correlation into account in deriving a new detection scheme: Such an issue can be adequately addressed in a future

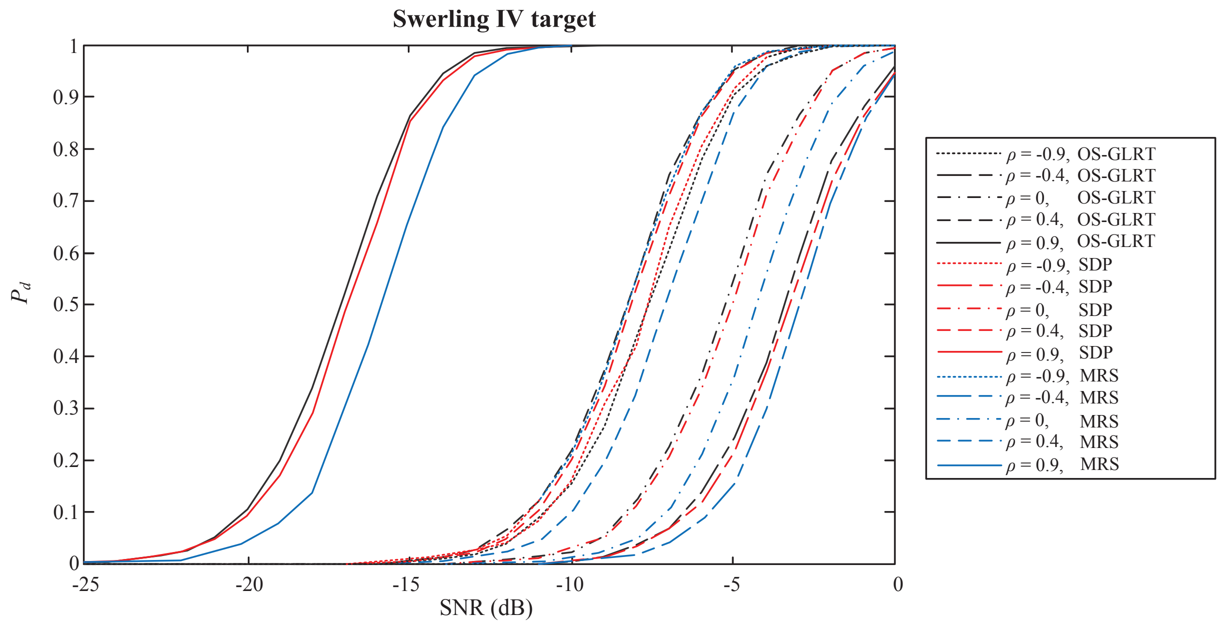

Fig. 4. Detection probability of the OS-GLRT, SDP, and MRS detectors for Swerling IV target.

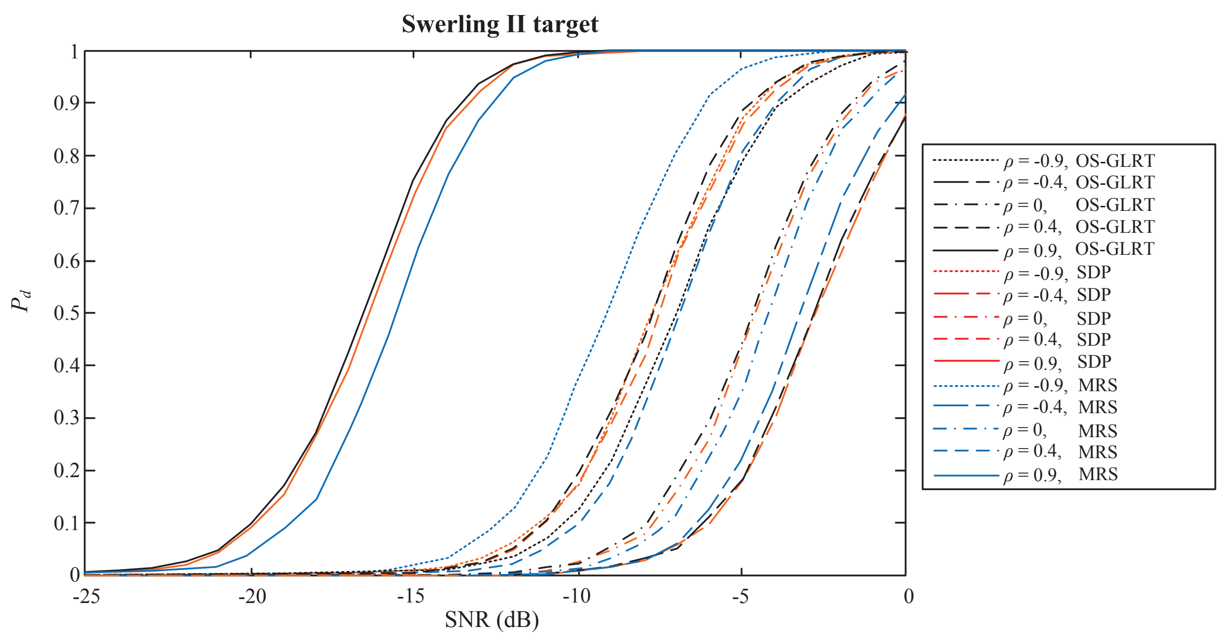

Fig. 5. Detection probability of the OS-GLRT, SDP, and MRS detectors for Swerling II target.

study.

IV. Conclusion

We have derived, and addressed the characteristics of, two detectors for the detection of a range-spread target with unknown Doppler frequency in Gaussian noise. First, the SDP detector is obtained from the maximization over the space of unknown Doppler frequency. Next, in an effort to reduce the complexity of the SDP, we have derived the MRS detector by adopting maximization over a reduced space. Both the SDP and MRS detectors can be applied even when exact knowledge of Doppler frequency is unavailable.

Performance characteristics of the two detectors proposed in this paper have been assessed in comparison with those of the conventional detector derived under the assumption of known Doppler frequency. When exact knowledge of Doppler frequency is available, the SDP and MRS detector is shown to provide detection performance comparable to that of the conventional detector at higher and similar complexity, respectively. If exact knowledge of Doppler frequency is unavailable, both the SDP and MRS detectors perform better than the conventional detector. At a slight performance loss in most cases, the MRS detector consumes much less processing time than the SDP detector. Under some circumstances including

This article has been accepted for publication in a future issue of this journal, but has not been fully edited. Content may change prior to final publication. Citation information: DOI 10.1109/TAES.2018.2847980, IEEE Transactions on Aerospace and Electronic Systems

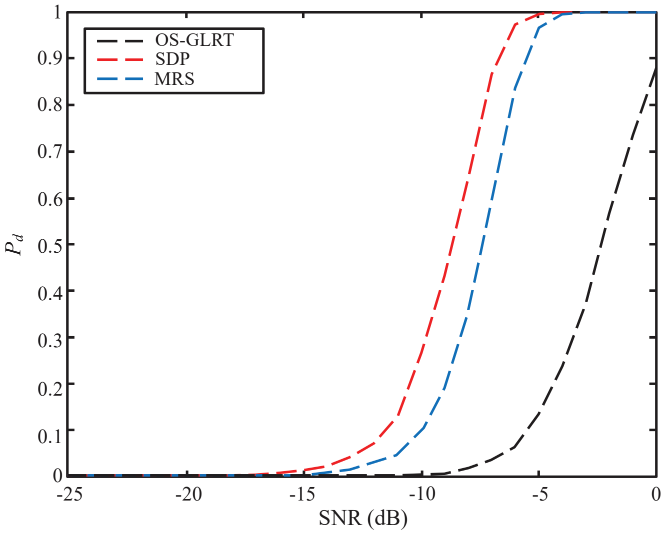

Fig. 6. Detection probability of the OS-GLRT, SDP, and MRS detectors for steady target when the information about the velocity of the target is not correctly provided.

the case of a high degree of fluctuation in range-spread targets, the MRS detector also outperforms the SDP and conventional detector.

Appendix A
Proof of the proposed GLRT (18)

Let us first show the equality

$$\left(\boldsymbol{Z}-\boldsymbol{p}\hat{\boldsymbol{\alpha}}^T\right)^H \boldsymbol{S}^{-1}\left(\boldsymbol{Z}-\boldsymbol{p}\hat{\boldsymbol{\alpha}}^T\right)=\boldsymbol{\Upsilon}-\kappa\left(\boldsymbol{p}\right)\boldsymbol{u}\boldsymbol{u}^H, \quad (48)$$

where

$$\boldsymbol{u}=\boldsymbol{Z}^H\boldsymbol{S}^{-1}\boldsymbol{p}. \quad (49)$$

If we expand the left-hand side of (48), we have

$$\begin{aligned}\left(\boldsymbol{Z}-\boldsymbol{p}\hat{\boldsymbol{\alpha}}^T\right)^H \boldsymbol{S}^{-1}\left(\boldsymbol{Z}-\boldsymbol{p}\hat{\boldsymbol{\alpha}}^T\right)&=\boldsymbol{\Upsilon}-\hat{\boldsymbol{\alpha}}^*\boldsymbol{p}^H\boldsymbol{S}^{-1}\boldsymbol{Z}\\&-\boldsymbol{Z}^H\boldsymbol{S}^{-1}\boldsymbol{p}\hat{\boldsymbol{\alpha}}^T+\frac{1}{\kappa\left(\boldsymbol{p}\right)}\hat{\boldsymbol{\alpha}}^*\hat{\boldsymbol{\alpha}}^T \quad (50)\end{aligned}$$

using (15) and (16). Next, we have $\hat{\boldsymbol{\alpha}}^*=\kappa\left(\boldsymbol{p}\right)\boldsymbol{Z}^H\boldsymbol{S}^{-1}\boldsymbol{p}=\kappa\left(\boldsymbol{p}\right)\boldsymbol{u}$ from (15) and (49) since $\kappa\left(\boldsymbol{p}\right)$ is a real number and $\boldsymbol{S}^{-1}$ is a Hermitian matrix. Thus, the second, third, and last terms in the right-hand side of (50) can be expressed as

$$\hat{\boldsymbol{\alpha}}^*\boldsymbol{p}^H\boldsymbol{S}^{-1}\boldsymbol{Z} \;=\; \kappa\left(\boldsymbol{p}\right)\boldsymbol{u}\boldsymbol{u}^H, \quad (51)$$

$$\boldsymbol{Z}^H\boldsymbol{S}^{-1}\boldsymbol{p}\hat{\boldsymbol{\alpha}}^T \;=\; \boldsymbol{u}\hat{\boldsymbol{\alpha}}^T, \quad (52)$$

and

$$\frac{1}{\kappa\left(\boldsymbol{p}\right)}\hat{\boldsymbol{\alpha}}^*\hat{\boldsymbol{\alpha}}^T \;=\; \boldsymbol{u}\hat{\boldsymbol{\alpha}}^T, \quad (53)$$

respectively. It is straightforward to get (48) using (51)-(53) in (50).

Now, noting that $|\boldsymbol{A}\boldsymbol{B}|=|\boldsymbol{A}|\,|\boldsymbol{B}|$ for square matrices $\boldsymbol{A}$ and $\boldsymbol{B}$ of the same size [32] and that $|\boldsymbol{I}_m+\boldsymbol{A}\boldsymbol{B}|=|\boldsymbol{I}_n+\boldsymbol{B}\boldsymbol{A}|$ for any $m\times n$ matrix $\boldsymbol{A}$ and $n\times m$ matrix $\boldsymbol{B}$ [34], the numerator in the left-hand side of (17) can be expressed as

$$\begin{aligned}\left|\boldsymbol{R}\left(\boldsymbol{0}_{L\times 1}\right)+\boldsymbol{S}\right| &= \left|\boldsymbol{S}\left(\boldsymbol{I}_N+\boldsymbol{S}^{-1}\boldsymbol{Z}\boldsymbol{Z}^H\right)\right|\\ &= |\boldsymbol{S}|\,|\boldsymbol{I}_L+\boldsymbol{\Upsilon}|\\ &= |\boldsymbol{S}|\,|\boldsymbol{X}|\,. \quad (54)\end{aligned}$$

Following similar steps, the term $|\boldsymbol{R}\left(\hat{\boldsymbol{\alpha}}\right)+\boldsymbol{S}|$ in the denominator of the left-hand side of (17) can be rewritten as

$$\begin{aligned}|\boldsymbol{R}\left(\hat{\boldsymbol{\alpha}}\right)+\boldsymbol{S}| &= \left|\boldsymbol{S}+\left(\boldsymbol{Z}-\boldsymbol{p}\hat{\boldsymbol{\alpha}}^T\right)\left(\boldsymbol{Z}-\boldsymbol{p}\hat{\boldsymbol{\alpha}}^T\right)^H\right|\\ &= |\boldsymbol{S}|\left|\boldsymbol{I}_L+\left(\boldsymbol{Z}-\boldsymbol{p}\hat{\boldsymbol{\alpha}}^T\right)^H\boldsymbol{S}^{-1}\left(\boldsymbol{Z}-\boldsymbol{p}\hat{\boldsymbol{\alpha}}^T\right)\right|. \quad (55)\end{aligned}$$

Subsequently, if we rewrite (55) with the result (48), we have

$$\begin{aligned}|\boldsymbol{R}\left(\hat{\boldsymbol{\alpha}}\right)+\boldsymbol{S}| &= |\boldsymbol{S}|\left|\boldsymbol{X}-\kappa\left(\boldsymbol{p}\right)\boldsymbol{u}\boldsymbol{u}^H\right|\\ &= |\boldsymbol{S}|\,|\boldsymbol{X}|\left|\boldsymbol{I}_L-\kappa\left(\boldsymbol{p}\right)\boldsymbol{X}^{-1}\boldsymbol{u}\boldsymbol{u}^H\right|\\ &= |\boldsymbol{S}|\,|\boldsymbol{X}|\left(1-\kappa\left(\boldsymbol{p}\right)\boldsymbol{u}^H\boldsymbol{X}^{-1}\boldsymbol{u}\right). \quad (56)\end{aligned}$$

From (54) and (56), we get (18) after a few straightforward steps.

Appendix B
Detailed steps from (19) to (22) and (23)

The maximization problem (18) and (19) can be recast as

$$\max_{\theta}\tilde{h}(\theta)\underset{H_0}{\overset{H_1}{\gtrless}}G_2, \quad (57)$$

where

$$\tilde{h}(\theta)=\frac{\boldsymbol{p}^H\boldsymbol{S}^{-1}\boldsymbol{Z}\boldsymbol{X}^{-1}\boldsymbol{Z}^H\boldsymbol{S}^{-1}\boldsymbol{p}}{\boldsymbol{p}^H\boldsymbol{S}^{-1}\boldsymbol{p}}. \quad (58)$$

For notational brevity, let us denote by a_{lm} and $[e_{lm}]_{k\times n}$ the element of $\boldsymbol{S}^{-1}\boldsymbol{Z}\boldsymbol{X}^{-1}\boldsymbol{Z}^H\boldsymbol{S}^{-1}$ at the l-th row and m-th column and a matrix of size $k\times n$ with elements $\{e_{lm}\}$, respectively. The numerator of $\tilde{h}(\theta)$ can then be expressed as

$$\begin{aligned}&\left[e^{-j(l-1)\theta}\right]_{1\times N}\left[a_{lm}\right]_{N\times N}\left[e^{j(m-1)\theta}\right]_{N\times 1}\\&=\sum_{l=1}^{N}\sum_{m=1}^{N}a_{lm}e^{-j(l-m)\theta}. \quad (59)\end{aligned}$$

Now, changing the summation index from $\{l,m\}$ to $\{l,k\}$ with $m-l=k$ and recollecting that $\left\{e^{-jk\theta}\right\}^*=e^{jk\theta}$ and $a^*_{l+k,l}=a_{l,l+k}$, from (59) we have

$$\begin{aligned}&\sum_{l=1}^{N}\sum_{m=1}^{N}a_{lm}e^{-j(l-m)\theta}\\&=\sum_{l=1}^{N}a_{ll}+\sum_{k=1}^{N-1}\sum_{l=1}^{N-k}\left(a_{l,l+k}e^{jk\theta}+a_{l+k,l}e^{-jk\theta}\right)\\&=x_0+\sum_{k=1}^{N-1}\left(e^{jk\theta}\sum_{l=1}^{N-k}a_{l,l+k}+e^{-jk\theta}\sum_{l=1}^{N-k}a^*_{l,l+k}\right)\\&=x_0+\sum_{k=1}^{N-1}2\mathcal{R}e\left\{x_k e^{jk\theta}\right\}, \quad (60)\end{aligned}$$

This article has been accepted for publication in a future issue of this journal, but has not been fully edited. Content may change prior to final publication. Citation information: DOI 10.1109/TAES.2018.2847980, IEEE Transactions on Aerospace and Electronic Systems

where

$$x_k = \sum_{l=1}^{N-k} a_{l,l+k} \tag{61}$$

for $k = 0, 1, ..., N-1$. With similar steps for the denominator also, (58) can eventually be rewritten as

$$\tilde{h}(\theta) = \frac{x_0 + 2\mathcal{R}e\left\{\sum\limits_{k=1}^{N-1} x_k \exp(jk\theta)\right\}}{y_0 + 2\mathcal{R}e\left\{\sum\limits_{k=1}^{N-1} y_k \exp(jk\theta)\right\}}, \tag{62}$$

where

$$y_k = \sum_{l=1}^{N-k} b_{l,l+k} \tag{63}$$

for $k = 0, 1, ..., N-1$ with $\{b_{lm}\}$ the elements of $\boldsymbol{S}^{-1}$. Now, let us denote the maximum of $\tilde{h}(\theta)$ by t. Then we have

$$\frac{x_0 + 2\mathcal{R}e\left\{\sum\limits_{k=1}^{N-1} x_k \exp(jk\theta)\right\}}{y_0 + 2\mathcal{R}e\left\{\sum\limits_{k=1}^{N-1} y_k \exp(jk\theta)\right\}} \leq t, \tag{64}$$

from which we can obtain (22) and (23) after some manipulations.

Appendix C
Proof of the CFAR property of the LRT (43)

The CFAR property of the LRT (43) will here be proven by showing that the distribution of the maximum eigenvalue $d_{\max}$ of $\boldsymbol{\Upsilon}$ under the null hypothesis is independent of the noise covariance matrix.

Let us first decompose the noise covariance matrix $\boldsymbol{C}$ as $\boldsymbol{C} = \boldsymbol{U}_C^H \boldsymbol{\Lambda}_C \boldsymbol{U}_C$, where $\boldsymbol{U}_C$ is an $N \times N$ unitary matrix such that $\boldsymbol{U}_C^{-1} = \boldsymbol{U}_C^H$ and $\boldsymbol{\Lambda}_C$ is the $N \times N$ diagonal matrix composed of the eigenvalues of $\boldsymbol{C}$. Next, define

$$\tilde{\boldsymbol{Z}} = \boldsymbol{Q}^{-1}\boldsymbol{Z} \tag{65}$$

and

$$\tilde{\boldsymbol{Z}}_S = \boldsymbol{Q}^{-1}\boldsymbol{Z}_S, \tag{66}$$

where $\boldsymbol{Q} = \boldsymbol{U}_C^H \boldsymbol{\Lambda}_C^{1/2} \boldsymbol{U}_C$ with $\boldsymbol{\Lambda}_C^{1/2}$ denoting the $N \times N$ diagonal matrix of the square roots of the diagonal elements of $\boldsymbol{\Lambda}_C$: Obviously, the diagonal elements of $\boldsymbol{\Lambda}_C$ are all positive since $\boldsymbol{C}$ is a positive definite matrix. Then, under the null hypothesis, we have $\tilde{\boldsymbol{Z}} = \left[\boldsymbol{Q}^{-1}\boldsymbol{n}_1, \boldsymbol{Q}^{-1}\boldsymbol{n}_2, \ldots, \boldsymbol{Q}^{-1}\boldsymbol{n}_L\right]$ and $\tilde{\boldsymbol{Z}}_S = \left[\boldsymbol{Q}^{-1}\boldsymbol{n}_{L+1}, \boldsymbol{Q}^{-1}\boldsymbol{n}_{L+2}, \ldots, \boldsymbol{Q}^{-1}\boldsymbol{n}_{L+K}\right]$: Thus, for any column of $\tilde{\boldsymbol{Z}}$ and $\tilde{\boldsymbol{Z}}_S$, we have

$$\begin{aligned} E\left[\left(\boldsymbol{Q}^{-1}\boldsymbol{n}_j\right)\left(\boldsymbol{Q}^{-1}\boldsymbol{n}_j\right)^H\right] &= \boldsymbol{Q}^{-1} E\left[\boldsymbol{n}_j \boldsymbol{n}_j^H\right] \left(\boldsymbol{Q}^{-1}\right)^H \\ &= \boldsymbol{Q}^{-1}\boldsymbol{C}\left(\boldsymbol{Q}^{-1}\right)^H \\ &= \boldsymbol{I}_N, \end{aligned} \tag{67}$$

which implies that the distributions of $\tilde{\boldsymbol{Z}}$ and $\tilde{\boldsymbol{Z}}_S$ do not depend on $\boldsymbol{C}$.

Next, the matrix $\boldsymbol{\Upsilon}$ can be rewritten as

$$\begin{aligned} \boldsymbol{\Upsilon} &= \tilde{\boldsymbol{Z}}^H \boldsymbol{Q}^H \left(\boldsymbol{Q}\tilde{\boldsymbol{Z}}_S \tilde{\boldsymbol{Z}}_S^H \boldsymbol{Q}^H\right)^{-1} \boldsymbol{Q}\tilde{\boldsymbol{Z}} \\ &= \tilde{\boldsymbol{Z}}^H \left(\tilde{\boldsymbol{Z}}_S \tilde{\boldsymbol{Z}}_S^H\right)^{-1} \tilde{\boldsymbol{Z}} \end{aligned} \tag{68}$$

from

$$\boldsymbol{S} = \boldsymbol{Z}_S \boldsymbol{Z}_S^H = \boldsymbol{Q}\tilde{\boldsymbol{Z}}_S \tilde{\boldsymbol{Z}}_S^H \boldsymbol{Q}^H. \tag{69}$$

It is therefore clear that, under the null hypothesis, the distribution of the maximum eigenvalue $d_{\max}$ of $\boldsymbol{\Upsilon}$ does not depend on the noise covariance matrix $\boldsymbol{C}$.

Acknowledgment

This work was supported by the National Research Foundation of Korea under Grant NRF-2018R1A2A1A05023192 with funding from the Ministry of Science and Information and Communication Technology, for which the authors wish to express their appreciation. The authors would also like to thank the Associate Editor and two anonymous reviewers for their constructive suggestions and helpful comments.

References

[1] D. Middleton, *An Introduction to Statistical Communication Theory*, New York, USA: McGraw-Hill, 1960.
[2] J. B. Thomas, *An Introduction to Communication Theory and Systems*, New York, USA: Springer-Verlag, 1988.
[3] R. N. McDonough and A. D. Whalen, *Detection of Signals in Noise*, Second Edition, New York, USA: Academic, 1995.
[4] I. Song, J. Bae, and S. Y. Kim, *Advanced Theory of Signal Detection*, Berlin, Germany: Springer-Verlag, 2002.
[5] M. I. Skolnik, *Radar Handbook*, Third Edition, New York, USA: McGraw-Hill, 2008.
[6] N. Bon, A. Khenchaf, and R. Garello, "GLRT subspace detection for range and Doppler distributed targets," *IEEE Trans. Aerosp., Electron. Syst.,* vol. 44, no. 2, pp. 678-696, Apr. 2008.
[7] K. Gerlach and M. J. Steiner, "Fast converging adaptive detection of Doppler-shifted, range-distributed targets," *IEEE Trans. Signal Process.,* vol. 48, no. 9, pp. 2686-2690, Sep. 2000.
[8] E. Conte, A. D. Maio, and G. Ricci, "GLRT-based adaptive detection algorithms for range-spread targets," *IEEE Trans. Signal Process.,* vol. 49, no. 7, pp. 1336-1348, July 2001.
[9] E. Conte, A. D. Maio, and C. Galdi, "CFAR detection of multidimensional signals: An invariant approach," *IEEE Trans. Signal Process.,* vol. 51, no. 1, pp. 142-151, Jan. 2003.
[10] A. D. Maio, A. Farina, and K. Gerlach, "Adaptive detection of range spread targets with orthogonal rejection," *IEEE Trans. Aerosp., Electron. Syst.,* vol. 43, no. 2, pp. 738-752, Apr. 2007.
[11] Y. He, T. Jian, F. Su, C. Qu, and X. Gu, "Novel range-spread target detectors in non-Gaussian clutter," *IEEE Trans. Aerosp., Electron. Syst.,* vol. 46, no. 3, pp. 1312-1327, July 2010.
[12] W. Liu, W. Xie, and Y. Wang, "Rao and Wald tests for distributed targets detection with unknown signal steering," *IEEE Signal Process. Lett.,* vol. 20, no. 11, pp. 1086-1089, Nov. 2013.
[13] Y. Gao, H. Li, and B. Himed, "Knowledge-aided range-spread target detection for distributed MIMO radar in nonhomogeneous environments." *IEEE Trans. Signal Process.,* vol. 65, no. 3, pp. 617-627, Feb. 2017.
[14] S. Kraut, L. L. Scharf, and L. T. McWhorterer, "Adaptive subspace detectors," *IEEE Trans. Signal Process.,* vol. 49, no. 1, pp. 1-16, Jan. 2001.
[15] G. A. Fabrizio, A. Farina, and M. D. Turley, "Spatial adaptive subspace detection in OTH radar," *IEEE Trans. Aerosp., Electron. Syst.,* vol. 39, no. 4, pp. 1407-1428, Oct. 2003.
[16] O. Besson and L. L. Scharf, "CFAR matched direction detector," *IEEE Trans. Signal Process.,* vol. 54, no. 7, pp. 2840-2844, July 2006.
[17] F. Bandiera, A. D. Maio, A. S. Greco, and G. Ricci, "Adaptive radar detection of distributed targets in homogeneous and partially homogeneous noise plus subspace interference," *IEEE Trans. Signal Process.,* vol. 55, no. 4, pp. 1223-1237, Apr. 2007.

[18] A. Aubry, A. D. Maio, D. Orlando, and M. Piezzo, “Adaptive detection of point-like targets in the presence of homogeneous clutter and subspace interference,” *IEEE Signal Process. Lett.,* vol. 21, no. 7, pp. 848-852, July 2014.

[19] W. Liu, W. Xie, and J. Liu, “Robust GLRT approaches to signal detection in the presence of spatial-temporal uncertainty,” *Signal Process.,* vol. 118, pp. 272-284, Jan. 2016.

[20] D. Ciuonzo, A. D. Maio, and D. Orlando, “A unifying framework for adaptive radar detection in homogeneous plus structured interference–Part II: Detectors design,” *IEEE Trans. Signal Process.,* vol. 64, no. 11, pp. 2907-2919, Nov. 2016.

[21] D. Ciuonzo, A. D. Maio, and D. Orlando, “On the statistical invariance for adaptive radar detection in partially homogeneous disturbance plus structured interference,” *IEEE Trans. Signal Process.,* vol. 65, no. 5, pp. 1222-1234, May 2017.

[22] S. Ramprashad, T. W. Parks, and R. Shenoy, “Signal modeling and detection using cone classes,” *IEEE Trans. Signal Process.,* vol. 4, no. 2, pp. 329-338, Feb. 1996.

[23] F. Bandiera, A. D. Maio, and G. Ricci, “Adaptive CFAR radar detection with conic rejection,” *IEEE Trans. Signal Process.,* vol. 55, no. 6, pp. 2533-2541, June 2007.

[24] A. D. Maio, S. D. Nicola, Y. Huang, S. Zhang, and A. Farina, “Adaptive detection and estimation in the presence of useful signal and interference mismatches,” *IEEE Trans. Signal Process.,* vol. 57, no. 2, pp. 436-450, Feb. 2009.

[25] F. Bandiera, D. Orlando, and G. Ricci, “CFAR detection strategies for distributed targets under conic constraints,” *IEEE Trans. Signal Process.,* vol. 57, no. 9, pp. 3305-3316, Sep. 2009.

[26] A. Svensson and A. Jakobsson, “Adaptive detection of a partly known signal corrupted by strong interference,” *IEEE Signal Process. Lett.,* vol. 18, no. 12, pp. 729-732, Dec. 2011.

[27] E. J. Kelly, “An adaptive detection algorithm,” *IEEE Trans. Aerosp., Electron. Syst.,* vol. 22, no. 1, pp. 115-127, Mar. 1986.

[28] E. J. Kelly and K. Forsythe, “Adaptive detection and parameter estimation for multidimensional signal models,” Lincoln Lab., Mass. Inst., Technol., Lexington, USA, Tech. Rep. no. 848, Apr. 1989.

[29] T. Roh and L. Vandenberghe, “Discrete transforms, semidefinite programming and sum-of-squares representations of nonnegative polynomials,” *SIAM J. Optim.,* vol. 16, no. 4, pp. 939-964, Jan. 2006.

[30] L. Vandenberghe and S. Boyd, “Semidefinite programming,” *SIAM Review,* vol. 38, no. 1, pp. 49-95, Mar. 1996.

[31] A. D. Maio, S. D. Nicola, A. Farina, and S. Iommelli, “Adaptive detection of a signal with angle uncertainty,” *IET Radar, Sonar, Navigation,* vol. 4, no. 4, pp. 537-547, Aug. 2010.

[32] G. H. Golub and C. F. V. Loan, *Matrix Computations*, Fourth Edition, Baltimore, MD: Johns Hopkins University Press, 2012.

[33] Y. Saad, *Numerical Methods for Large Eigenvalue Problems: Revised Edition,* Philadelphia, USA: SIAM, 2011.

[34] R. A. Horn and C. R. Johnson, *Matrix Analysis*, Second Edition, New York, USA: Cambridge University Press, 2012.

[35] H. A. David and H. N. Nagaraja, *Order Statistics*, Third Ed., New York, NY, USA: John Wiley and Sons, 2003.

[36] I. Song, C.H. Park, K.S. Kim, and S.R. Park, *Random Variables and Stochastic Processes* (in Korean), Paju, Korea: Freedom Academy, 2014.

[37] A. Lepoutre, O. Rabaste, and F. L. Gland, “Multitarget likelihood computation for track-before-detect applications with amplitude fluctuations of type Swerling 0, 1, and 3,” *IEEE Trans. Aerosp., Electron. Syst.*, vol. 52, no. 3, pp. 1089-1107, June 2016.

[38] Y. Nesterov and A. Nemirovskii, *Interior-Point Polynomial Algorithms in Convex Programming*, Philadelphia, PA, USA: SIAM, 1994.

[39] Z.-Q. Luo and W. Yu, “An introduction to convex optimization for communications and signal processing,” *IEEE J. Sel. Areas Commun.*, vol. 24, no. 8, pp. 1426-1438, Aug. 2006.

[40] C. Shen, J. Kim, F. Liu, L. Wang, and A. v. d. Hengel, “Efficient Dual Approach to Distance Metric Learning,” *IEEE Trans. Neural Netw., Learn. Syst.*, vol. 25, no. 2, pp. 394-406, Feb. 2014.

Seungwon Lee received the B.S.E. degree in electronics engineering from Kyung Hee University, Yongin, Korea, in 2010, and the M.S.E. degree in electrical engineering from Korea Advanced Institute of Science and Technology (KAIST), Daejeon, Korea, in 2012. He is currently working toward the Ph.D. degree at KAIST. Since February 2010, he has been a Teaching and Research Assistant in the School of Electrical Engineering, KAIST. His research interests include mobile communications, detection and estimation theory, and statistical signal processing.

Mai Nguyen received the bachelor degree in Telecommunications from Da Nang University of Science and Technology, Vietnam, in 2010, and the M.S.E. degree in electrical engineering from Korea Advanced Institute of Science and Technology (KAIST), Daejeon, Korea, in 2015. Since 2015, she has been a Ph.D. student in the School of Electrical Engineering, KAIST. Her research interests include radar signal processing, compressed sensing, and machine learning.

Iickho SONG (S’80-M’87-SM’96-F’09) received the B.S.E. (*magna cum laude*) and M.S.E. degrees in electronics engineering from Seoul National University, Seoul, Korea, in 1982 and 1984, respectively, and the M.S.E. and Ph.D. degrees in electrical engineering from the University of Pennsylvania, Philadelphia, PA, USA, in 1985 and 1987, respectively. He was a Member of the Technical Staff at Bell Communications Research in 1987. In 1988, he joined the School of Electrical Engineering, Korea Advanced Institute of Science and Technology, Daejeon, Korea, where he is currently a Professor. He has coauthored a few books including *Advanced Theory of Signal Detection* (Springer, 2002) and *Random Variables and Random Processes* (Freedom Academy, 2014; in Korean), and published papers on signal detection, statistical signal processing, and applied probability. Prof. Song is a Fellow of the Korean Academy of Science and Technology (KAST). He is also a Fellow of the IEEE and IET, and a Member of the Acoustical Society of Korea (ASK), Institute of Electronics Engineers of Korea (IEEK), Korean Institute of Communications and Information Sciences (KICS), Korea Institute of Information, Electronics, and Communication Technology, and Institute of Electronics, Information, and Communication Engineers. He has served as the Treasurer of the IEEE Korea Section, an Editor of the *Journal of the ASK*, an Editor of *Journal of the IEEK*, an Editor of the *Journal of the KICS*, an Editor of the *Journal of Communications and Networks (JCN)*, and a Division Editor of the *JCN*. He has received several awards including the Young Scientists Award (KAST, 2000), Achievement Award (IET, 2006), and Hae Dong Information and Communications Academic Award (KICS, 2006).

Jinsoo Bae (S’93-M’98-SM’03) was born in Seoul, Korea in 1972. He received the Ph.D. degrees in electrical engineering from Korea Advanced Institute of Science and Technology (KAIST), Daejeon, Korea, in 1998. In March 2000, he joined the Department of Electrical Engineering, Sejong University, Seoul, Korea, where he is currently a Professor. His research interests include nonparametric detection theory. Dr. Bae is a Senior Member of the IEEE.

This article has been accepted for publication in a future issue of this journal, but has not been fully edited. Content may change prior to final publication. Citation information: DOI 10.1109/TAES.2018.2847980, IEEE Transactions on Aerospace and Electronic Systems

Seokho Yoon (S'99-M'02-SM'07) received the Ph.D. degrees in electrical engineering from Korea Advanced Institute of Science and Technology (KAIST), Daejeon, Korea, in 2002. In March 2003, he joined the College of Information and Communication Engineering, Sungkyunkwan University, Suwon, Korea, where he is currently a Professor. His research interests include mobile communications and detection and estimation theory. Dr. Yoon is a Senior Member of the IEEE.

FIGURE CAPTIONS

Fig. 1. False alarm probability versus thresholds of the SDP detector.

Fig. 2. Detection probability of the OS-GLRT, SDP, and MRS detectors for steady target.

Fig. 3. Detection probability of the OS-GLRT, SDP, and MRS detectors for steady target.

Fig. 4. Detection probability of the OS-GLRT, SDP, and MRS detectors for Swerling IV target.

Fig. 5. Detection probability of the OS-GLRT, SDP, and MRS detectors for Swerling II target.

Fig. 6. Detection probability of the OS-GLRT, SDP, and MRS detectors for steady target when the information about the velocity of the target is not correctly provided.